Applied Thermal Engineering 195 (2021) 117187

Contents lists available at ScienceDirect

Applied Thermal Engineering

journal homepage: www.elsevier.com/locate/apthermeng

Multi-objective optimization of a chip-attached micro pin fin liquid cooling system

Vahideh Radmard [a,*], Yaser Hadad [a], Srikanth Rangarajan [a], Cong H. Hoang [a], Najmeh Fallahtafti [a], Charles L. Arvin [b], Kamal Sikka [b], Scott N. Schiffres [a], Bahgat G. Sammakia [a]

[a] Department of Mechanical Engineering, State University of New York at Binghamton, Binghamton, NY, USA
[b] IBM, NY, USA

ARTICLE INFO

Keywords:
High heat flux chip
Jet Impingement
TIM
Direct cooling
Chip-attached micro pin fin
Regression
Multi-objective optimization

ABSTRACT

This study explores heat transfer from a chip-attached micro pin fin cooling device undergoing water jet impingement where the silicon chip is in direct contact with the cooling liquid. Directly attaching the micro pin fins onto the chip surface is a new packaging technique that eliminates the contact and sequential conduction resistance of thermal interfaces, which are still used in conventional electronic packages. A multi-objective optimization is solved to minimize the cooling device's thermal resistance and pressure drop as response parameters. The influence of design parameters, such as pin fin cross section, fin spacing and the fin height profile, on the response parameters is investigated using computational fluid dynamics (CFD) and full factorial design of experiment (FFD). The optimization study is accomplished in two parts. In the first part, the shape optimization is performed by a traditional weighted sum approach using an iterative JAYA algorithm. The shape optimization problem is also solved using modern optimization algorithm of NSGA-II. The results of both approaches are in a close agreement. In the second part, an optimization of the fin height profile is solved using an Artificial Neural Network (ANN) combined with an elitist NSGA-II. The overall analysis demonstrates that the optimized cooling device can surpass its initial working design in thermal and hydraulic performance. Hence, there is excellent potential for the use of lightweight and compact designs in Heterogeneous Integration (HI) applications.

1. Introduction

For the electronics industry, one major problem continues to be the excess heat generated from high-power electronic devices, which acts as a bottleneck to their performance and lifespan. Numerous articles have been written detailing the limits of cooling techniques for electronic systems including [1–7]. The most viable thermal solution is the use of heat exchangers with extended surfaces. Heat sinks that are well-designed can meet the heat dissipation requirement for the high heat flux of electronic devices at a reduced chip temperature. Recently, much effort has been dedicated to the analysis of heat transfer and flow performance of liquid cooled pin fin heatsinks. The liquid cooled heat sinks can be performed in an indirect or direct contact with coolant and with parallel or impinging inlet based on the required application. One promising approach to enhancing heat transfer is the use of jet impingement cooling devices. Impingement's enhancement of heat transfer has been well established through years of study, research, and experience in a wide range of applications. Several studies have been developed for jet impingement schemes with regard to the effects of jet pattern and jet geometry [8–15]. Naphon et al. experimentally studied indirect (coolant is not in direct contact with the silicon chip) jet nano fluid impingement heat transfer and pressure drop features in a micro-channel heat sink. In their parametric study, the authors concluded that the thermal performance improved with decreasing jet nozzle level height and increasing nozzle diameter, while the pressure drop increased with increasing nozzle level height and decreasing nozzle diameter [16]. In another study Naphon et al. [17] experimentally investigated jet liquid impingement cooling in a rectangular pin fin channel heat sink for central processing unit (CPU) of personal computers applications. The authors concluded that the jet liquid impingement cooling device has a better thermal performance than the conventional liquid system.

In the case of indirect liquid cooling, cold plate heat sinks require the cooling device to be attached to the chip using a thermal interface material (TIM), of which there are several types depending on the application. Accordingly, the challenge for thermal engineers is to lower the thermal resistance resulting from contact and conduction of TIMs. For

* Corresponding author.
E-mail address: vradmar1@binghamton.edu (V. Radmard).

https://doi.org/10.1016/j.applthermaleng.2021.117187
Received 7 December 2020; Received in revised form 22 April 2021; Accepted 1 June 2021
Available online 7 June 2021

Nomenclature

A	Area (m^2)
A_r	Ration of jet orifice area and chip area
b	Height of pin fin at the center of assemblage(m)
C_1	Turbulent model constant
C_2	Turbulent model constant
c_p	Specific heat capacity ($J/kg.K$)
D_h	Hydraulic diameter (m)
H	Separation height between jet nozzle and chip surface(m)
H_{full}	Maximum height of pin fin before shortening(m)
h	Heat transfer coefficient $\left(\frac{W}{K}m^2\right)$
k	Thermal conductivity ($J/m.K$)
k	Turbulent kinetic energy(m^2/s^2)
$\dot{m}$	Mass flow rate (kg/s)
Nu	Nusselt number
P	Pressure (Pa)
Q	Coolant volumetric flow rate (m^3/s)
$\dot{q}$	Chip power (W)
R_{th}	Thermal resistance ($K.m^2/W$)
Re	Reynolds number
s	Spacing(m)
T	Temperature (K)
t	Thickness of pin fin (m)
u	Velocity (m/s)
V	Volume(m^3)
x	Coordinate(m)

Greek symbols

ε	Turbulent energy dissipation rate
μ	Absolute viscosity ($kg/m.s$)
μ_t	Eddy viscosity
Ξ	Objective function
ξ	Weight factor
ρ	Density (kg/m^3)
ψ	Chip temperature non-uniformity
ϵ	Porosity
σ_k	Diffusion Prandtl number for k
θ	Profile slope($radian$)

Subscripts

ch	chip
e	External
f	Pin fin
i	Internal
in	Inlet
$J-ch$	Junction to chip
l	Liquid
S	Solid
TIM	Thermal interface material
th	Thermal

this purpose, one approach is using high thermal conductivity TIMs such as silver pastes and indium [18]. However, previous simulations [19–22] indicated that even high conductivity TIMs might not be able to keep up with high heat fluxes as thermal resistances become extremely large. Another approach is direct liquid cooling performs in jet impingement scheme, which eliminates the need for TIMs and delivers the coolant directly onto the surface of the chip. Wu et al. [23] investigated and analyzed a direct jet impingement body cooling device and a channel/jet impingement hybrid body cooling device with micro-nozzles through a thermal model. Their result showed there exists a critical nozzle diameter that determines which device has better cooling performance. Their thermal model was in good agreement with the experiment results. Iyengar et al. [24] studied and numerically analyzed the thermal and hydraulic performance of a square silicon chip (1 cm × 1 cm) dissipating 400W in a direct liquid multi-jet impingement scheme.

One shortcoming of the conventional jet impingement design is the lower heat transfer area. A few studies proposed introducing enhanced structures such as extended surfaces to improve the performance of jet impingement cooling device. Wiriyasart et al. [25] experimentally and numerically investigated the cooling performance of an indirect liquid jet impinged heat sink cold plate with different pin fin geometries (rectslope, circle, cone). Their designed cold plate was capable of cooling a high heat flux of over 500 Wover a small heating area of 4 cm × 4 cm. Ndao et al. [26] experimentally showed that crossflow has no significant effect on the heat transfer coefficients for a single-phase impingement micro-device by adding pin fins. However, the authors did find that augmenting the heat transfer area significantly enhanced the overall heat transfer. The results showed that of the various micro pin fin geometries, the circular and square pin fins had the highest heat transfer coefficient. Peles et al. [27] studied heat transfer and pressure drop phenomena over a bank of micro pin fins. Based on their results, the thermo-hydraulic performance of flow across a microscale cylindrical pin fin array is superior to plain microchannel based cooling.

In recent years, it has been indicated that selective laser melting (SLM) can be used to fabricate enhanced structures directly onto a silicon chip without the need for conventional TIMs [19,20]. In this process a Sn-Ag-Ti interlayer alloy is used to bond silicon die to the metal structures. Subsequently, an alloy with high conductivity, such as copper or aluminum, can be printed on top of the interlayer alloy using a powder bed fusion technique to create heat sinks. Conrad et al. showed that using the SLM approach, metallic pin fins pointing towards the chip can be printed on top of an electronic chip without violating electronic functionality. The authors showed that SLM direct printed pin approach can provide lower thermal resistance in a smaller volume, reduce plastic strain and improve reliability of cooling device in comparison to state-of-the-art actively cooled power modules such as Hybridpack 2 of Infineon [28,29].

Recently, many studies have extensively used design of experiment methods (DOE) in conjunction with computational fluid dynamics (CFD) with various optimization algorithms to optimize cooling devices with different geometries [30–32]. Li and Kim [16] applied a multi-objective optimization technique using the genetic algorithm (GA) to optimize a pin fin array using three-dimensional Reynolds averaged Navier–Stokes (RANS) equations with the shear-stress transport (SST) turbulence model. In their analysis with response surface method (RSM), the second-order polynomial was utilized as a response surface [33]. The RSM with CFD and sequential approximation optimization (SAO) method were used by Chiang et al. [34] to find the optimal values for design parameters of an impinging pin fin type heat sink under design constraints and to obtain the best cooling performance. Kasza et al. [35] applied a particle swarm optimization (PSO) algorithm for the neural network training to perform a design optimization of a staggered pin fin impinging heat sink made of a thermally conductive polymer. The authors investigated the effect of design parameters (pin fin height, the diameter, or the number of pins) on the thermal performance of the natural convection heat sink was studied. Negi et al. [36] used RSM and multi-objective Genetic Algorithm to optimize the profile of dimples on the target surface in a multi-jet impingement heat transfer device. They used CFD to calculate response parameters of the average Nusselt number, maximum Nusselt number, and deviation of maximum Nusselt number from the average value.

ANN and GA were extensively employed for optimizing cooling system designs [37–39]. Horiuchi et al. [40] studied geometric optimization of a water-cooled pin fin heat sink considering low pressure drop, high heat transfer rate, and manufacturability. They used GA and empirical equations to obtain Pareto-optimal trade-off curves. Eghtesad et al. [41] optimized the cooling performance of twin turbulent sweeping impinging jets. They used artificial neural network (ANN) combined with genetic algorithm (GA) to evaluate the optimal values of the jet design parameters. A geometrical optimization method for changing pin fin porosity and pin fin slope was proposed by Zhao et al. [42]. The efficiency of various multi objective optimization algorithms coupled with artificial neural networks were discussed in [43]. The authors concluded the NSGA-II and traditional genetic algorithm is highly efficient when coupled with ANN based regression for highly nonlinear problems.

In the present study, jet impingement direct liquid cooled chip attached micro pin fin cooling device is proposed to increase value of term heat transfer coefficient (h) and heat transfer surface area (A). This increase is attributed to the larger heat transfer area between solid and liquid portions, and enhancement of the heat transfer coefficient, h, due to the depression of the thermal boundary layer growth and flow mixing. This approach can provide more functionality in a smaller packaging space, which will help overcome existing space limitations for heterogeneous integration applications. There is still room to investigate an impinged direct liquid cooling device with an enhanced pin fin structure, especially when it comes to the effect of pin fin geometry and the fin heigh profile on the device's heat transfer and fluid flow behavior. To the best of authors' knowledge, there is no study that reports a multi-objective optimization of chip-attached micro pin fin heat sink undergoing direct water jet impingement. Therefore, a new combined technique to enhance heat transfer is optimized and explored computationally in this paper. This work is complementary to a previous published study [44] which numerically studied the effect of outlet port position on the hydraulic and thermal performance of the pin fin chip-attached cooling design. An optimization study is done to examine the effects of pin fin geometry (pin fin cross section and fin spacing) and the fin height profile on the thermal resistance and pressure drop of the cooling device. A parametric study is presented for the design parameters. At the conclusion, optimum solutions to the objective functions are illustrated. Additionally, the rules derived from this study are expected to help designers build cooling devices that operates with an improved performance while remaining within its specified temperature range.

2. Problem description

The schematic diagram of predefined geometry is illustrated in Fig. 1. It is worth mentioning that the size of the components is exaggerated to facilitate a better understanding of the model. Starting at the bottom layer, a silicon chip with a specified uniform heat flux is placed on the bottom of the design. Micro pin fins with square cross sections are fabricated on the surface of a silicon chip. The unique aspect of this design is printing pin fins onto the chip surface and removing TIM and spreader. The coolant is collected at the periphery of the chip through four outlets with specified dimensions, which are in the lower part of plastic sidewalls. At the top layer, a plastic lid contains an inlet sits on the setup. As shown in the Fig. 1, the coolant is impinged down through the inlet port placed on the top surface of the configuration. The uniform velocity and the constant temperature are imposed at the inlet. Geometric and operational parameters are listed in Table 1 and Table 2, respectively.

The heat flow in typical heat sinks depends on conduction from the electronic package to the heat sink base, followed by conduction into the heat sink surface and convection to the flow. In electronic cooling for a heat sink, the total thermal resistance is the sum of the individual resistances, as given by:

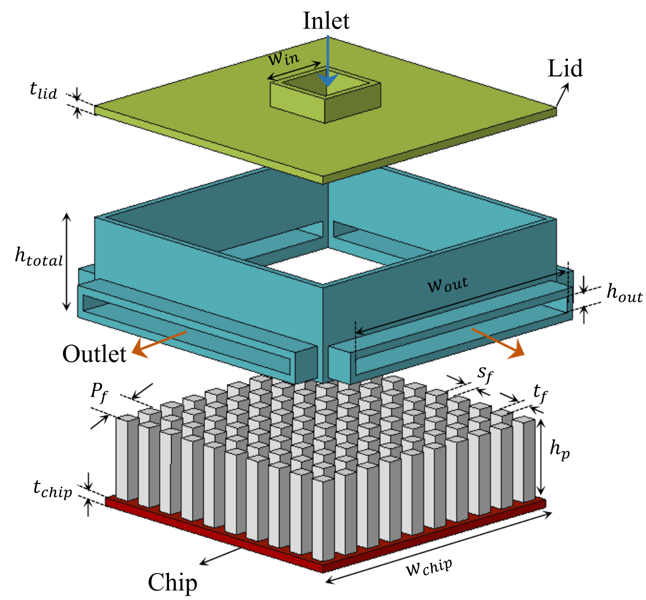

Fig. 1. A schematic diagram of the assemblage with geometric parameters.

Table 1
Geometric parameters of the predefined design with their values in mm.

Symbol	Definition	Value (mm)
h_f	Pin fin height	5
h_{out}	Outlet port height	0.8
h_{total}	Total height	5.7
w_{chip}	Chip width	20
w_{out}	Outlet width	19.5
w_{in}	Inlet width	3
t_{chip}	Chip thickness	0.2
t_{lid}	Lid thickness	2
P_f	Pin fin pitch	0.8
t_f	Thickness of pin fin	0.4
s_f	fin spacing	0.4

Table 2
Operational parameters of the module with their values.

Symbol	Definition	Value
T_{in}	Coolant inlet temperature	300 (K)
$\dot{q}_{Chip}$	Chip total power	500 (W)
A_{Chip}	Chip area	400 (mm^2)
Q	Coolant flow rate	83.33(cm^3/s)

$$R_{th}^{tot} = R_i + R_e \tag{1}$$

The internal resistance constitutes the sum of resistances:

$$R_i = R_{j-ch} + R_{TIM} + R_{spreading} \tag{2}$$

The advantage of printing cooling structure directly onto a chip is to remove internal resistance caused by TIM and spreader.

2.1. Materials properties

The coolant used in the current study is dielectric water with an inlet temperature of 300 K (Table 3). Since this is a numerical study of a design that is going to be manufactured using 3D printing, silver was chosen for printing micro pin fins, as it is easier to print. Thermo-

Table 3
Thermo-physical properties of the coolant and soli.

	$c_p\left(\frac{J}{kg.K}\right)$	$k\left(\frac{W}{m.K}\right)$	$\rho\left(\frac{kg}{m^3}\right)$	$\mu\left(\frac{kg}{m.s}\right)$
Coolant	4179	0.613	997	0.00085
Silver	230	406	10,500	–
Copper	385	401	8978	–
TIM	1000	3	2500	–

physical properties of silver at room temperature (300 k) were obtained from the thermodynamics tables. Considering that the printing volume is small, so the cost is not unreasonable. These trends and general geometry also are applicable to copper and aluminum.

3. Methodology

The influence of geometric parameters, such as pin fin cross section, fin spacing, and fin height profile on the thermal and hydraulic performance of the cooling device are calculated numerically through full factorial design of experiment (FFD). Based on numerical data at FFD design points, a multi objective geometric optimization is performed in two parts (Sections 4.1 and 4.2). In the first part, optimization of pin fin cross section, fin spacing is performed as shape optimization to minimize the thermal resistance and pressure drop of the cooling device. The optimization is accomplished using a traditional weighted sum approach using an iterative JAYA algorithm and modern optimization algorithm of NSGA-II. In the second part, fin height profile optimization is done using an Artificial Neural Network (ANN) combined with an elitist NSGA-II. To conduct CFD results, the finite-volumes method is applied as a discretization technique to solve the system of governing equations. A mapped structured grid with hexahedral cells is applied to discretize the computational domain. The fin space are subjected to finer grids due to higher temperature and velocity gradients in these regions. SIMPLE algorithm is employed as the iterative method to solve governing equations and represent the field functions of pressure, velocity, and temperature. The commercial program 6Sigma ET is incorporated as the numerical solver. The stop residual for the function of temperature is set to 0.0001 as a convergence criterion. The residual of the other functions, k, ε, velocity and pressure are 0.0005. The following are the basic assumptions made to numerically model all designs in this study.

- The flow is assumed to be three dimensional, incompressible, and steady.
- The buoyancy and radiation heat transfer effects are negligible.
- The thermo-physical properties of the solid and coolant are assumed to be constant.
- Viscous heat generation is negligible.
- The flow is turbulent.

3.1. Governing equations

The turbulent three-dimensional governing equations for a three dimensional, incompressible, steady-state condition are used to simulate the thermal and turbulent flow fields. The $k-\varepsilon$ model is used to describe turbulent effects. The three-dimensional governing equations of continuity, momentum, turbulent kinetic energy, turbulent energy dissipation rate, and energy in the steady turbulent main flow are provided in this section:

Conservation of mass equation:

$$\frac{\partial \rho_f \overline{u}_i}{\partial x_i} = 0 \tag{3}$$

Navier-Stokes equation for the liquid phase:

$$\rho_f \overline{u}_j \frac{\partial \overline{u}_i}{\partial x_j} = -\frac{\partial p}{\partial x_i} + \frac{\partial}{\partial x_j}\left[(\mu+\mu_t)\left(\frac{\partial \overline{u}_i}{\partial x_j} + \frac{\partial \overline{u}_j}{\partial x_i}\right)\right] \tag{4}$$

Energy equation for the liquid phase:

$$\rho_f \overline{u}_j \frac{\partial \overline{T}}{\partial x_j} = \frac{\partial}{\partial x_j}\left[\left(\frac{\mu_l}{\sigma_l} + \frac{\mu_t}{\sigma_T}\right)\frac{\partial \overline{T}}{\partial x_j}\right] \tag{5}$$

Energy equation for the solid phase:

$$\frac{\partial}{\partial x_i}\left[k_s \frac{\partial T}{\partial x_i}\right] = 0 \tag{6}$$

Turbulent kinetic energy equation:

$$\rho \overline{u}_j \frac{\partial k}{\partial x_j} = \frac{\partial}{\partial x_j}\left[\left(\mu + \frac{\mu_t}{\sigma_k}\right)\frac{\partial k}{\partial x_j}\right] + \mu_t\left[\frac{\partial \overline{u}_i}{\partial x_j} + \frac{\partial \overline{u}_j}{\partial x_i}\right]\frac{\partial \overline{u}_i}{\partial x_j} - \rho\varepsilon \tag{7}$$

Turbulent energy dissipation rate equation:

$$\rho \overline{u}_j \frac{\partial \varepsilon}{\partial x_j} = \frac{\partial}{\partial x_j}\left[\left(\mu + \frac{\mu_t}{\sigma_\varepsilon}\right)\frac{\partial \varepsilon}{\partial x_j}\right] + C_1\mu_t\frac{\varepsilon}{k}\left[\frac{\partial \overline{u}_i}{\partial x_j} + \frac{\partial \overline{u}_j}{\partial x_i}\right]\frac{\partial \overline{u}_i}{\partial x_j} - C_2\rho\frac{\varepsilon^2}{k} \tag{8}$$

Where $\sigma_k = 1$ and $\sigma_\varepsilon = 1.30$.

Finally, the Reynolds number of the impinging jet is given by:

$$\mathrm{Re} = \frac{\rho u_{in} D_h}{\mu_l} \tag{9}$$

The value of the Re number is calculated at inlet is equal to 32×10^3.

3.2. Numerical domain and boundary conditions

The computational domain is reduced to one-quarter of the whole assemblage using the advantage of symmetry in both geometry and heat flux boundary conditions. A schematic description of the physical domain, including boundary conditions, is shown in Fig. 2. Again, the proportions of the figure are exaggerated for clarity. The zero gradients are applied in two planes of symmetry, which are shown with black dashed lines. At the velocity inlet, the coolant is uniformly induced downward with a constant temperature and leaves the module from pressure outlets placed on the sides of the cold plate. Constant heat flux is applied to the chip area on the bottom of cooling device. No-slip hydraulic boundary condition is imposed along the heat sink walls, which are in contact with the fluid. All remaining outside surfaces are considered adiabatic.

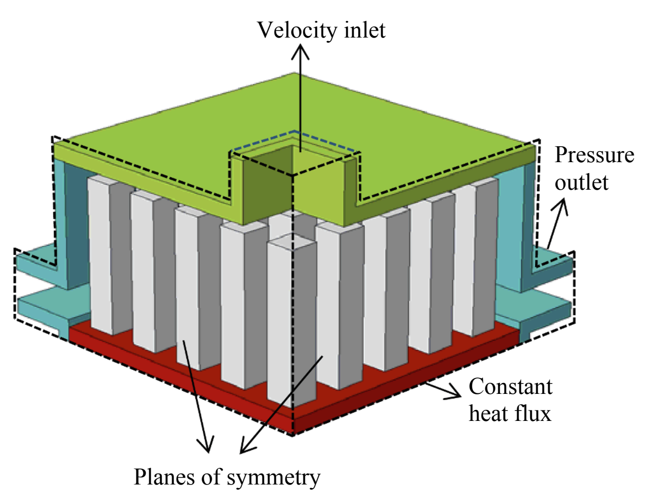

Fig. 2. A schematic view of the computational domain with applied boundary conditions.

3.3. Grid resolution analysis

The analysis of grid resolution is performed based on the pressure drop in the system and thermal resistance.

The result of the grid study (Fig. 3) depicts that increasing the number of cells from 11.7 million to 14.1 million leads to a 2.3% and 0.9% variation in the pressure drop and thermal resistance, respectively. All results reported subsequently have used approximately 11.7 million number of grid refinement.

4. Results and discussion

4.1. Optimization process

A multi-objective optimization study is conducted for thermal resistance and pressure drop. The maximum chip temperature of 343 K and a maximum pressure drop of 4 psi (27.6 kPa) are defined as operational design constraints.

4.1.1. Shape optimization

4.1.1.1. Design parameters. Thickness of pin fin (t_f) and fin spac (s_f) are design parameters for the shape optimization study. Values of t_f range from 0.3 to 0.6 mm, and the given range of variation for s_f is between 0.25 and 0.4.

4.1.1.2. Response parameters. Thermal resistance is often used as the main criterion for evaluating the efficiency of heat dissipation and rating the performance of the cooling device. The thermal resistance of the cooling device (R_{th}) can be defined by

$$R_{th} = \frac{T_{ch}^{Max} - T_{in}}{\dot{q}_{ch}} \tag{10}$$

In which, T_{ch}^{Max} and T_{in} are the maximum temperature of electronic chip and the inlet temperature of the coolant, respectively. $\dot{q}_{ch}$ is the total chip power applied to the chip.

The second response parameter in this study is the pressure(ΔP).

The method of four-level full factorial design of experiment (FFD) is used to investigate the relative effects of the design parameters on the thermal and hydraulic performance of the device. Sixteen design points were generated in the design space (Table 4). The thermal resistance and pressure drop of the device are calculated using CFD. In addition to the response parameters, the coefficient of variation is used to address the temperature distribution non-uniformity of the chip (Ψ) for each design point. It is defined by

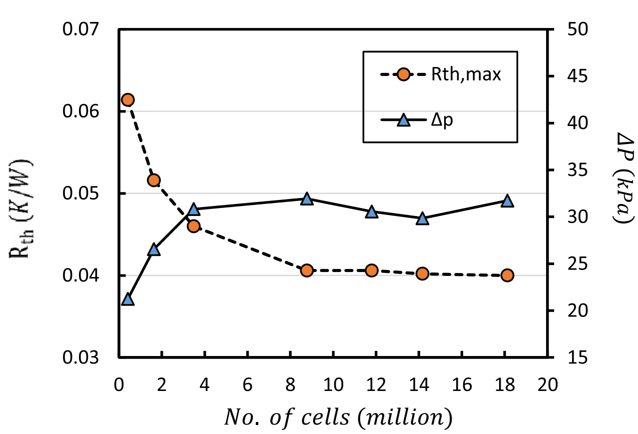

Fig. 3. The results of grid resolution based on thermal resistance and pressure drop.

Table 4
Calculated response parameters at FFD design points for shape optimization.

No	$t_f(mm)$	$s_f(mm)$	R_{th}(K/W)	$\Delta P(kPa)$	ψ
1	0.40	0.40	0.0406	31.50	0.78
2	0.40	0.25	0.0286	57.78	0.44
3	0.60	0.30	0.0294	61.47	0.40
4	0.40	0.35	0.0370	35.32	0.62
5	0.60	0.40	0.0352	39.85	0.61
6	0.60	0.35	0.0320	54.51	0.49
7	0.50	0.30	0.0306	56.15	0.45
8	0.30	0.40	0.0482	28.11	0.83
9	0.60	0.25	0.0268	80.91	0.39
10	0.30	0.35	0.0424	30.43	0.68
11	0.30	0.30	0.0364	41.61	0.59
12	0.50	0.35	0.0340	46.09	0.54
13	0.50	0.40	0.0382	37.58	0.66
14	0.50	0.25	0.0276	62.20	0.41
15	0.40	0.30	0.0324	49.39	0.52
16	0.30	0.25	0.0314	48.31	0.52

$$\Psi = \frac{\sqrt{\sum_{n=1}^{N} \frac{(T_n - T_{ave})^2}{N-1}}}{T_{ave}} \tag{11}$$

Where N is the number of points uniformly distributed on the electronic chip. In this study, the Ψ is obtained using temperature records from 121 points. The higher value of Ψ the chip has, the more non-uniform temperature distribution it gets.

4.1.1.3. Analysis of variance and regression. Regression analysis is employed to estimate the functions of thermal resistance and pressure drop in quadratic form.

$$R_{th} = 0.00942 - 0.0423t_f + 0.16354s_f + 0.0861{t_f}^2 - 0.1907t_f s_f \tag{12}$$

$$\Delta P = 4.4538 + 1.547t_f - 4.041s_f \tag{13}$$

Both R-squared (R^2) and adjusted R-squared values ($R^2(Adjusted)$) are obtained from ANOVA tables for each regression function. The values of $R^2$and $R^2(Adjusted)$ for R_{th} are 99.50% and 99.32%, respectively. Similarly, R^2 values of 96.88%, 96.40% are obtained for ΔP. The average relative error between the results of the regression model and CFD at design points FFD points are about 1.04% and 4.28% for R_{th} and ΔP, respectively.

In addition to statistical validation, the accuracy of the regression models of Eqs. (12) and (13) is confirmed using CFD simulation. To check the accuracy of the regression models, two intermediate points are chosen from the defined range of design parameters and compared with the prediction obtained from regression functions. As Table 5 shows the regression model predictions are in a good agreement with CFD simulation results.

4.1.1.4. Sensitivity analysis. Sensitivity analysis is a mathematical procedure to evaluate "how" and "how much" uncertainties in the design parameters and their interaction terms modify the optimal objective function value. The chart of Fig. 4 presents the effect of each design parameter term on the pressure drop and thermal resistance. Considering the design parameters range of variation and design conditions (fixed parameters), the inter-fin spacing has the highest contribution to both the thermal resistance (68%) and pressure drop (64%). The thickness of the micro pin fin plays as the second most important parameter in terms of pressure drop (36%). The interaction terms have no impact on the pressure drop.

4.1.1.5. Optimal designs. Multi-objective optimization is performed based on the designed heat sink. The design parameters (t_f ands_f) are optimized to minimize the pressure drop (ΔP) and thermal resistance of model (R_{th}). The optimization problem can be stated as:

Table 5
Confirmation of the regression models by CFD.

Design Parameters		$R_{th}(K/W)$			$\Delta P(kPa)$		
$t_f(mm)$	$s_f(mm)$	Simulation	Regression	Discrepancy	Simulation	Regression	Discrepancy
0.35	0.32	0.0358	0.0363	1.34%	40.14	40.32	0.47%
0.40	0.28	0.0302	0.0304	0.85%	51.45	52.25	1.56%

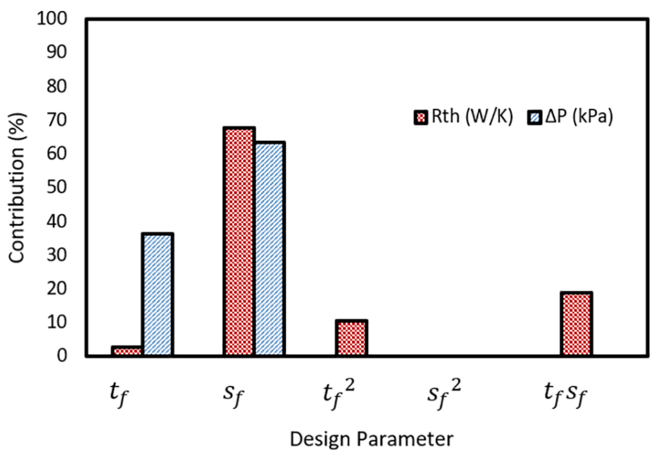

Fig. 4. The results of the sensitivity analysis showing the contribution of each design parameter term on the pressure drop and thermal resistance.

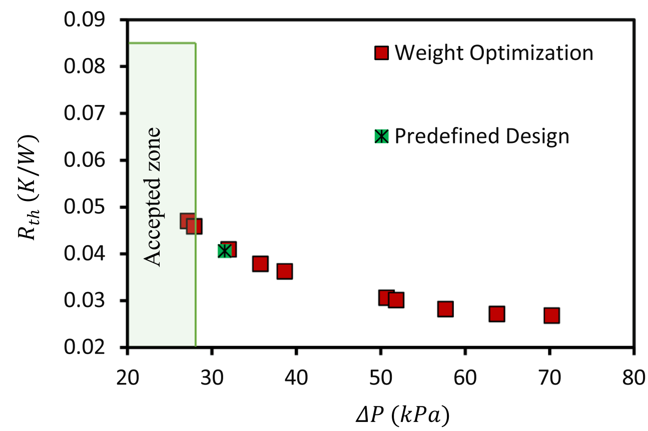

Fig. 5. The best trade off curve between thermal resistance and pressure drop obtained using weight optimization method in conjunction with Jaya iterative algorithm.

$$\text{Minimize}: R_{th} = f_1(t_f, s_f) \tag{14}$$

$$\text{Minimize}: \Delta P = f_2(t_f, s_f) \tag{15}$$

subjected to

$$0.3 \le t_f \le 0.6 \tag{16a}$$

$$0.25 \le s_f \le 0.4 \tag{16b}$$

Where, $f_1$and f_2 are mentioned regression models (Eqs. (12) and (13)) of the thermal resistance and pressure drop. The problem above is solved using a weight optimization approach. A combination of the response parameters is done to form a single objective function.

$$\Xi_{\Delta P-R_{th}} = \xi_{\Delta P}\left(\frac{\Delta P}{\Delta P^{min}}\right) + \xi_{R_{th}}\left(\frac{R_{th}}{R_{th}{}^{min}}\right) \tag{17}$$

Where, ΔP^{min} and $R_{th}{}^{min}$are the minimum values of regression functions of Eqs. (12) and (13). $\xi_{\Delta P}$ and $\xi_{R_{th}}$ are the weight factors ascribed to ΔP, and R_{th}, respectively. In an attempt to minimize the objective function, JAYA algorithm is used as a tool to provide optimal solutions. The best trade off curve or Pareto plot between thermal resistance and pressure drop are obtained using weight optimization method in conjunction with JAYA iterative algorithm. Additionally, the Pareto optimal points are generated using a non-dominated sorted Genetic Algorithms (NSGA II). The results are in close agreement with the results obtained from the weight sum approach. As shown in Fig. 5, there are two optimal points which have acceptable pressure drop. While all optimal points have acceptable thermal resistance. A profile optimization is developed to achieve designs with lower pressure drop values lie in accepted zone, keeping thermal resistance almost the same.

4.1.2. *Profile optimization*

4.1.2.1. Design parameters. Linear profile (Fig. 6) is selected for fin profile optimization. The slope (θ) and intercept (b) of the linear profile are considered as the optimization design parameters for the profile optimization study, in which each design parameter is defined in the given range of variation. The given range of variation for θ is between 0 and 0.48 rad (27.5°) and b can take values ranging from 0 to $0.84h_{full}$ ($0 \le \mathrm{b} \le 4.20$ mm). Note that when $\theta = 0$ and $\mathrm{b} = 0$ (minimum) there are no fins, and when $\theta = 0.48$ and $\mathrm{b} = 4.2$ (maximum) the pins are approximately at full height (Fig. 7).

4.1.2.2. Artificial neural networks. Using the four-level FFD method, sixteen design points are generated in the design space (Table 6). Accurate numerical simulations are conducted to study the effect of pin fin profile on the thermo-hydraulic performance of the chip attached micro pin fin cooling device. An Artificial Neural Network (ANN) was developed using MATLAB. ANN is a non-linear regression tool [45]. It comprises of an input layer, hidden layer, and output layer. In general, the number of hidden layers can be more than one. The relationship between input and output can be modelled using neural networks by training available sets of input and output data. A supervised learning [46] based ANN is employed in this study. The nodes in the hidden layers are represented by a function that can modify its weight during training. A typical structure of an ANN is depicted in Fig. 8.

The available set of output data is fed into the network (target data). The target data is divided into three data sets, namely the training set, validation set, and testing set. The training dataset is used to adjust the weights on the neural network. The validation data set is used to minimize the overfitting. The testing data set is used only for testing the final solution to confirm the actual predictive power of the network. In addition to this, ANN is tested using additional data from simulations. Among various algorithms employed to train the network, the back propagation training approach is widely used in the field of neural networking [29,30]. An ANN based on feedforward-back propagation was employed in this study. The fitting process was initialized with guess values for the initial weights and at every iteration, the error between the target data and the actual data was compared and minimized by employing optimal weights. The main objective of a neural network is to find the best set of weight coefficients so that the output neurons could closely represent the problem under consideration. During training, the offset between actual neural network outputs and desired outputs for all the training samples is computed iteratively to evaluate

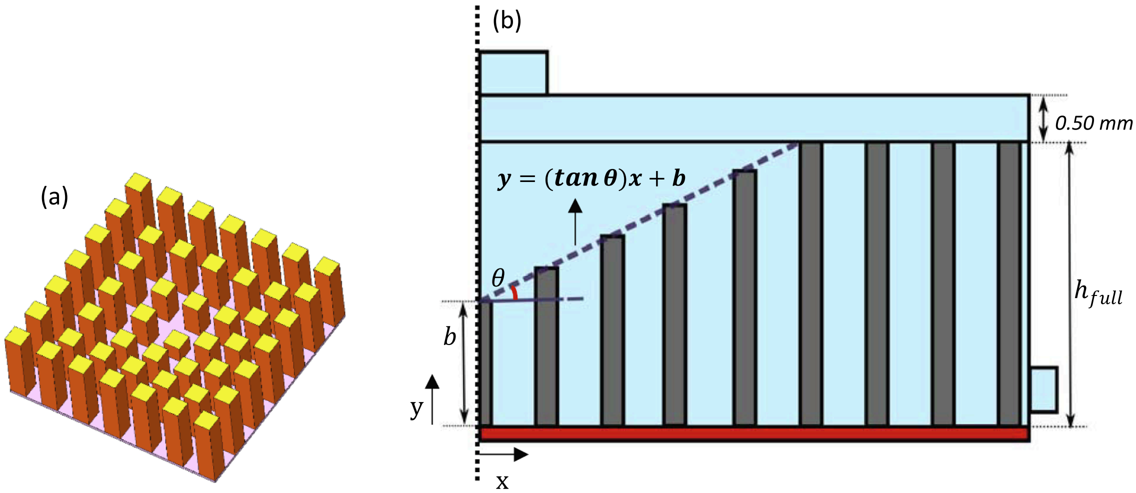

Fig. 6. a) A schematic of the device's fin height profile and b) assigned design parameters for a cross section of device.

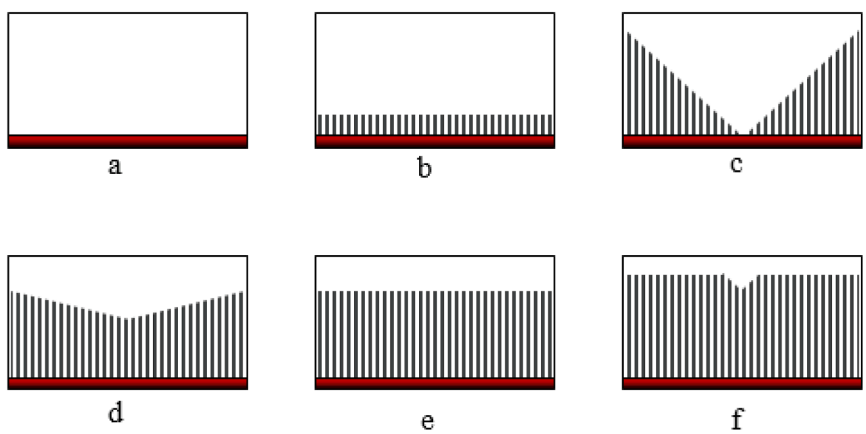

a) No pin-fin design with $\theta = 0\,rad$ and $b =$ 0 mm	d) Case design with $\theta = 0.16$ rad and $b = 2.8$ mm
b) Case design with $\theta = 0$ rad and $b = 1.4$ mm	e) Case design with $\theta = 0$ rad and $b = 4.2$ mm
c) Case design with $\theta = 0.48$ rad and $b =$ 0 mm	f) Full pin-fin design with $\theta = 0.48$ rad and $b =$ 4.2 mm

Fig. 7. Schematic of different designs with various fin profiles. a) No pin–fin design with $\theta = 0rad$ and $b = 0\mathrm{mm}$ b) Case design with $\theta = 0\mathrm{rad}$ and $b = 1.4\mathrm{mm}$ c) Case design with $\theta = 0.48\mathrm{rad}$ and $b = 0\mathrm{mm}$ d) Case design with $\theta = 0.16\mathrm{rad}$ and $b = 2.8\mathrm{mm}$ e) Case design with $\theta = 0\mathrm{rad}$ and $b = 4.2\mathrm{mm}$ f) Full pin–fin design with $\theta = 0.48\mathrm{rad}$ and.$b = 4.2\mathrm{mm}$

the performance of neural network. The iteration is continued until a stopping criterion is satisfied. In this study, the slope (θ) and intercept (b) of the linear profile are two independent variables that are fed into the input layer of the network. Furthermore, gradient descent is used to adjust weights and repeat the iteration until the error is minimized to the desired accuracy. The procedure for ANN in this study is as follows:

a) Select input and output parameters for the neurons in the input and output layer, respectively. In this study, the slope (θ) and intercept (b) are employed for the input layer while the thermal resistance and pressure drop are associated with the output layer.

b) Divide available data collected from the simulations into two types of training and testing data sets. 75% of the initial data is used for training.

c) Normalize the data, which is done in the range of [-1, 1] since the hyperbolic tangent function has its limiting values in the range [-1, 1].

d) Determine the optimal number of neurons using the neuron independent study. In this study the optimal number of neurons is calculated to be 4.

e)Set proper transfer functions for all layers. A hyperbolic tangent function is introduced into the hidden layers.

f) Train the network. This is done with the help of the Levenberg-Marquat method, which minimized the error to determine the optimal weights in the least square sense.

g) Introduce the learning rate of 0.01 initially, which will then change adaptively as the iterations progress.

h) Regression analysis of training and validation. One of the advantages of adopting an ANN is its efficiency to handle nonlinear trends in heat transfer problems over a conventional polynomial expression [43]. The results of the regression analysis for the problem under consideration is shown in the Fig. 9. The network's prediction and the actual numerical data are in good agreement.

In the early stage of the optimization process, the conflicting nature

Table 6
Calculated response parameters at FFD design points for profile optimization.

No	θ (rad)	b(mm)	R_{th}(K/W)	$\Delta P(kPa)$	ψ
1	0	1.4	0.0674	17.80	1.66
2	0.48	4.2	0.0438	29.56	0.77
3	0	0	0.0820	13.78	0.95
4	0	2.8	0.0548	19.18	1.16
5	0.32	1.4	0.0492	18.98	0.99
6	0.16	1.4	0.0588	18.53	1.29
7	0.48	0	0.0508	18.62	0.96
8	0.48	2.8	0.0438	21.37	0.77
9	0.32	2.8	0.0442	20.67	0.80
10	0.16	2.8	0.0476	19.71	0.93
11	0.32	0	0.0682	17.84	1.39
12	0.16	0	0.0704	17.39	1.27
13	0.48	1.4	0.0450	19.58	0.85
14	0	4.2	0.0464	23.98	0.87
15	0.32	4.2	0.0438	27.55	0.77
16	0.16	4.2	0.0438	25.85	0.78

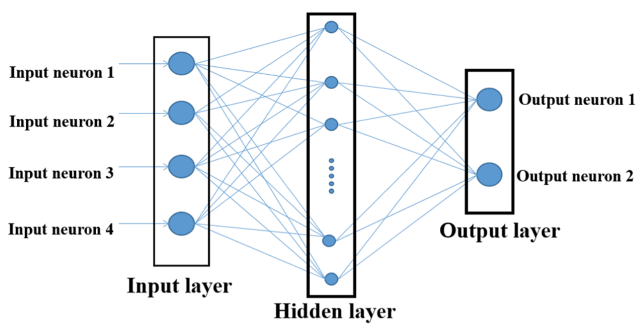

Fig. 8. Basic architecture of the neural network.

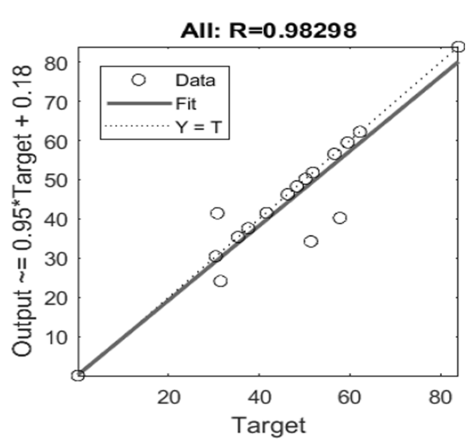

Fig. 9. Results of regression analysis using ANN.

of the objectives are evaluated. From Fig. 10, it is evident that the objectives are in a high degree of conflict throughout the variable search space generated from LHS. Therefore, a multi-objective optimization would be thoroughly helpful to obtain best trade off curves between objectives. The ANN model is coupled with genetic algorithm to obtain the set of Pareto optimal solutions.

4.1.2.3. Genetic algorithm. The highly conflicting nature of the objectives shown in Fig. 10, is a motivation to perform a multi-objective optimization. The resulting regression model from the ANN is employed as an objective function for the state-of-the-art optimization using non-nominated sorted genetic algorithm. The elitist non-dominated sorted genetic algorithm (NSGA), also known as NSGA-II

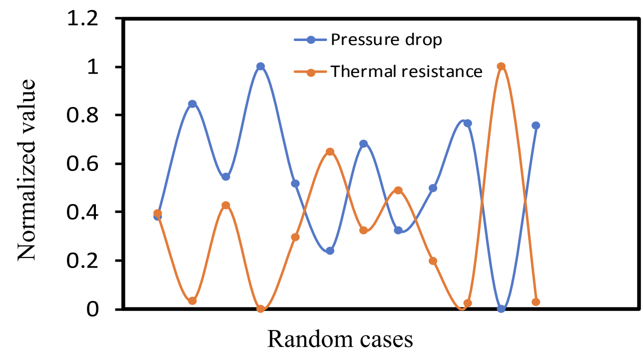

Fig. 10. Conflicting nature of the objective functions.

[29,30], is used to simultaneously optimize both objectives. Rudolph's elitist multi-objective evolutionary algorithm developed in 2001 implemented the elite (the term elite refers to solutions that have the highest objective function value, in the case of a maximization problem) preserving mechanism and the solutions converged to the true Pareto curve in a finite number of generations. In NSGA-II not only the elite members in each generation are carried over to the next generation, along with which diversity of the solution is also preserved in each generation. Diversity refers to the spread of the solution, which is more important to achieve the global optimum.

The output of the NSGA-II can be evaluated by two parameters.

- Closeness to true Pareto solution (Obtained from Brute force using LHS)
- Diversity in the solution

The initial points chosen for the algorithm are shown in Fig. 11. This process continues until either the maximum number of generations is reached, or a satisfactory fitness level is attained. The strong ability of the genetic algorithms to tackle the search spaces containing many local optimal is one of its attractive features for engineers. In contrary to the conventional search methods and calculus, genetic algorithms initiate the search at multiple number of points in the search space. The desired accuracy in the value of slope and intercept of the profile is chosen to be 2. Initial population is generated randomly, and its size is chosen as 30. Once the initial population is generated, the corresponding fitness value is evaluated, and ranking is done. Subsequently, operators like selection, crossover, and mutation are applied to the population as long as the Pareto optimal is obtained. Mutation is applied to all the individuals greater than or equal to the probability of mutation. The newly generated binary strings are converted to integers and then to the

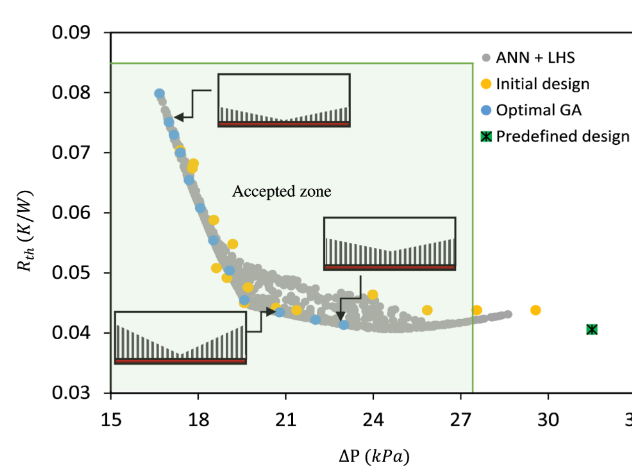

Fig. 11. Pareto optimal solution of the fin height profile optimization.

corresponding real number. The population number (N), generation/iteration count (G), probability of crossover (P_c) and probability of mutation (P_m) have been found after an extensive study. Finally, the parameters N = 30, G = 180, P_c=0.6, P_m=0.4 are achieved through a sensitivity study. A detailed procedure of NSGA-II can be found in [31]. Table 7 summarizes the Pareto optimal solutions obtained from NSGA-II. The Pareto plot provides optimal design models for a specific thermal and hydraulic requirement. The results of Pareto optimal solutions obtained from NSGA-II were confirmed by CFD (Table 7 & 8). The NSGA-II algorithm is seen to be superior to the available optimization algorithms in terms of diversity and spread of the solutions [43]. The algorithm is capable of identifying solutions from various regions of the Pareto curve without missing few global optimal solutions (Fig. 11). Also, NSGA-II inherently preserves the elite candidate in all the generations. The elite offspring are preserved through the generations and hence global optimal solutions are ensured. However, the disadvantage of NSGA-II could be that it is sensitive to the operation parameters (probability of mutation and probability of crossover) and requires a thorough sensitivity study to find the robust set of parameters of the algorithm.

Using profile optimization, it is possible to achieve a design with 37% less pressure drop than predefined design without scarifying thermal resistance. Based on the Pareto plot of Fig. 11, the optimal points remain within the defined pressure drop limit. In another word, profile optimization is an effective method to achieve design with lower pressure drop while remaining acceptable thermal resistance. This reduction in pressure drop is favorable as less pumping power and leak probability are achieved with the same thermal performance.

4.2. Model validation to Martin's correlation

Validation of the CFD results of the case model with no pin fins attached is performed using Martin's correlation [8,47]. To use Martin's correlation for a single nozzle, the following equations are recommended.

$$\frac{\overline{Nu}}{Pr^{0.42}} = G(A_r, H/D)F(Re) \tag{18a}$$

$$F(Re) = 2Re^{\frac{1}{2}}\left(1 + 0.005Re^{0.55}\right)^{\frac{1}{2}} \tag{18b}$$

$$G = 2A_r\frac{1 - 2.2A_r^{\frac{1}{2}}}{1 + 0.2\left(\frac{H}{D} - 6\right)A_r^{\frac{1}{2}}} \tag{18c}$$

In the recommended range of validity of

$$2000 \le Re \le 400000 \tag{19a}$$

$$2 \le \frac{H}{D_h} \le 12 \tag{19b}$$

$$0.04 \le A_r \le 0.004 \tag{19c}$$

The effective heat transfer coefficient from numerical modeling calculated by

$$\overline{h} = \frac{\dot{q}}{\left(T_{ave}^{chip} - T_{in}^{coolant}\right)} \tag{20}$$

is compared to average heat transfer coefficient predicted by Martin's correlation.

The heat transfer coefficient values of CFD and Martin's correlation are found to be 36337and 31176$\left(\frac{W}{cm^2}.K\right)$, respectively, which shows approximately a 14% discrepancy.

Table 7
Pareto optimal solution of the fin height profile optimization.

No	θ (rad)	b(mm)	R_{th}(K/W)	ΔP(kPa)
1	0.197	1.141	0.080	16.673
2	0.260	0.415	0.075	16.997
3	0.418	2.050	0.073	17.171
4	0.316	0.265	0.070	17.392
5	0.369	1.393	0.061	18.073
6	0.313	2.634	0.050	19.071
7	0.451	1.876	0.045	19.583
8	0.354	0.276	0.043	20.789
9	0.151	2.403	0.042	22.023
10	0.102	2.640	0.041	22.989
11	0.355	2.869	0.055	18.520
12	0.376	2.400	0.065	17.682
13	0.19	1.35	0.055	18.56
14	0.48	1.4	0.046	19.57

4.3. Interpretation of CFD results

To assess the sole effect of design parameters such as fin space, thickness of pin fins, and profile slope and intercept on the heat transfer and hydraulic performance of the system, three parameters are characterized:

1. Porosity is an important parameter that defines the percentage volume of voids constituted in a total volume. High porosity means that the volume that can be occupied by the fluid is high, and that the contact area available for the fluid flow is high. In the case of impingement design, flow area can be represented by the porosity,€ defined as:

$$\text{€} = \frac{V_{void}}{V_{total}} \tag{21}$$

2. Conduction thermal resistance of the pin fin is carried out for different design cases. It can be defined using Fourier's law:

$$R_{th}^{pin} = \frac{L_{pin}}{kA_{pin}} \tag{22}$$

Where L_{pin} and A_{pin} are height and cross section area on a single pin fin.

3. Additionally, the solid–liquid contact surface area is assessed for each case.

Fig. 12(a) depicts the variation of thermal resistance for different fin spacings and thicknesses. The thermal resistance at a fixed pin thickness of 0.30 mm, increases by 40% when increasing fin space from 0.25 to 0.40 mm. As Fig. 12(a) shows, for a fixed fin space, thermal resistance improves with an increase in the fin thickness. One explanation for this is that conduction resistance of a fin is inversely proportional to its thickness, thus thicker pins provide lower conduction resistance. Another explanation is that thicker pin fins with a fixed fin space offer a greater heat transfer surface area.

The pressure drop variation with t_f and s_f are shown in Fig. 12(b). The results manifests that for a fixed fin thickness, an increase in the fin spacing reduces the pressure drop because of the acquired higher porosity and lower velocity. Pressure drop is a function of velocity, solid–fluid contact surface area. As expected, thicker fins lead to a higher pressure drop because of higher velocity and solid–fluid contact surface area. The trends for temperature distribution non-uniformity generally show the same trends as thermal resistance (Fig. 12(c)). Aforementioned reasons for the dependency of thermal performance on design parameters can also explain the temperature distribution non-uniformity trends. The temperature profile of chip with a minimumΨ (t_f = 0.60,s_f = 0.25)

Table 8
Validation of the optimal points by CFD.

Design Parameters		$R_{th}(K/W)$			$\Delta P(kPa)$		
θ	b	Simulation	NSGA-II	Discrepancy	Simulation	NSGA-II	Discrepancy
0.19	1.35	0.0564	0.055	2.48%	18.50	18.56	0.30%
0.48	1.4	0.0450	0.046	2.2%	19.58	19.57	0.04%

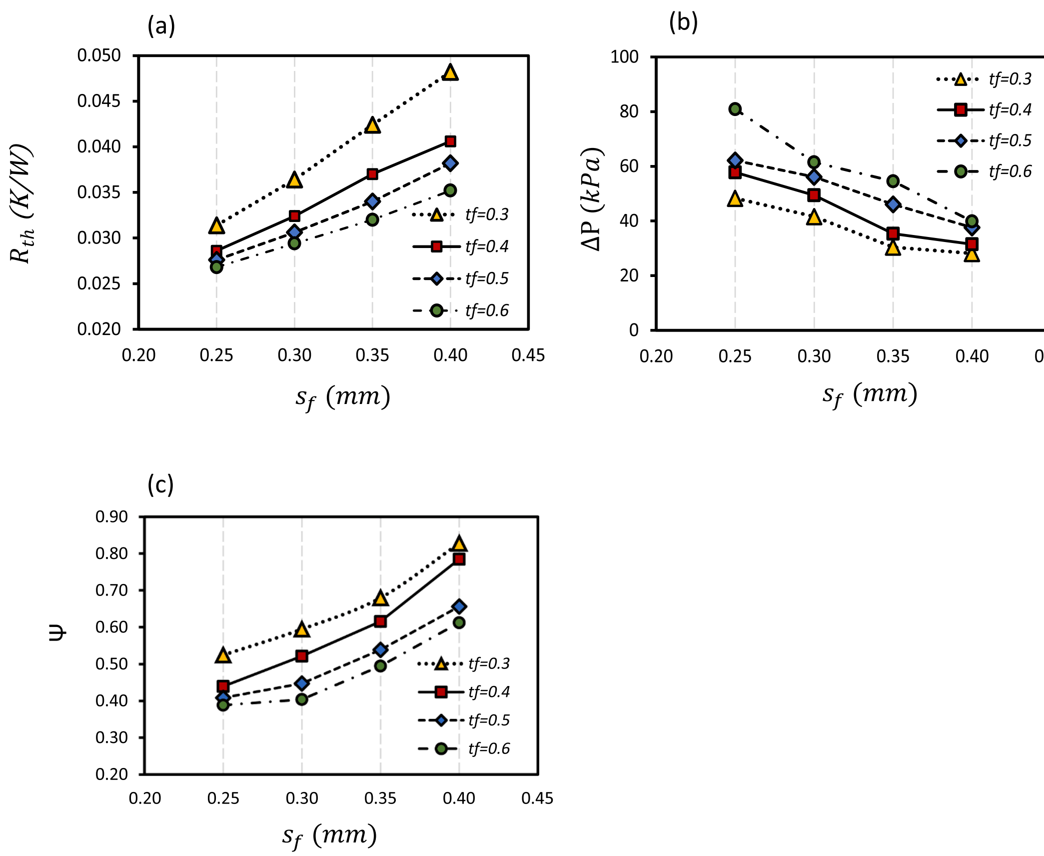

Fig. 12. The effect of the shape design parameters on the response parameters in the constant flow rate. (a) The effect of pin thickness and fin space on the thermal resistance. (b) The effect of pin thickness and fin space on the pressure drop. (c) The effect of pin thickness and fin space on the temperature distribution non-uniformity.

and maximum $\Psi(t_f = 0.3, s_f = 0.40)$ are compared in Fig. 13. It is concluded that geometric parameters can have a significant impact on the temperature uniformity of the chip circuit.

The effect of profile slope and intercept on the hydraulic and thermal performance of the device is shown in Fig. 14. With increasing slope value, thermal performance will improve due to the higher heat transfer surface area. As the Fig. 14(a) shows, for a design with a specified profile slope, the thermal resistance improves with an increase in the intercept due to higher heat transfer surface area. To be more specific, the thermal resistance trend for the profile with intercept of 4.20 mm did not show

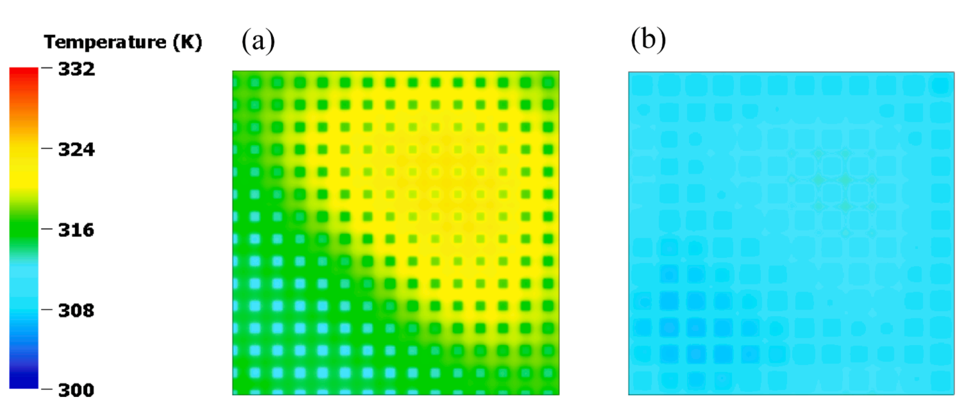

Fig. 13. Representative temperature profile on the chip surface, (a) Temperature profile for case design with maximum Ψ ($t_f = 0.3, s_f = 0.4$), (b) Temperature profile for case design with minimumΨ ($t_f = 0.6, s_f = 0.25$).

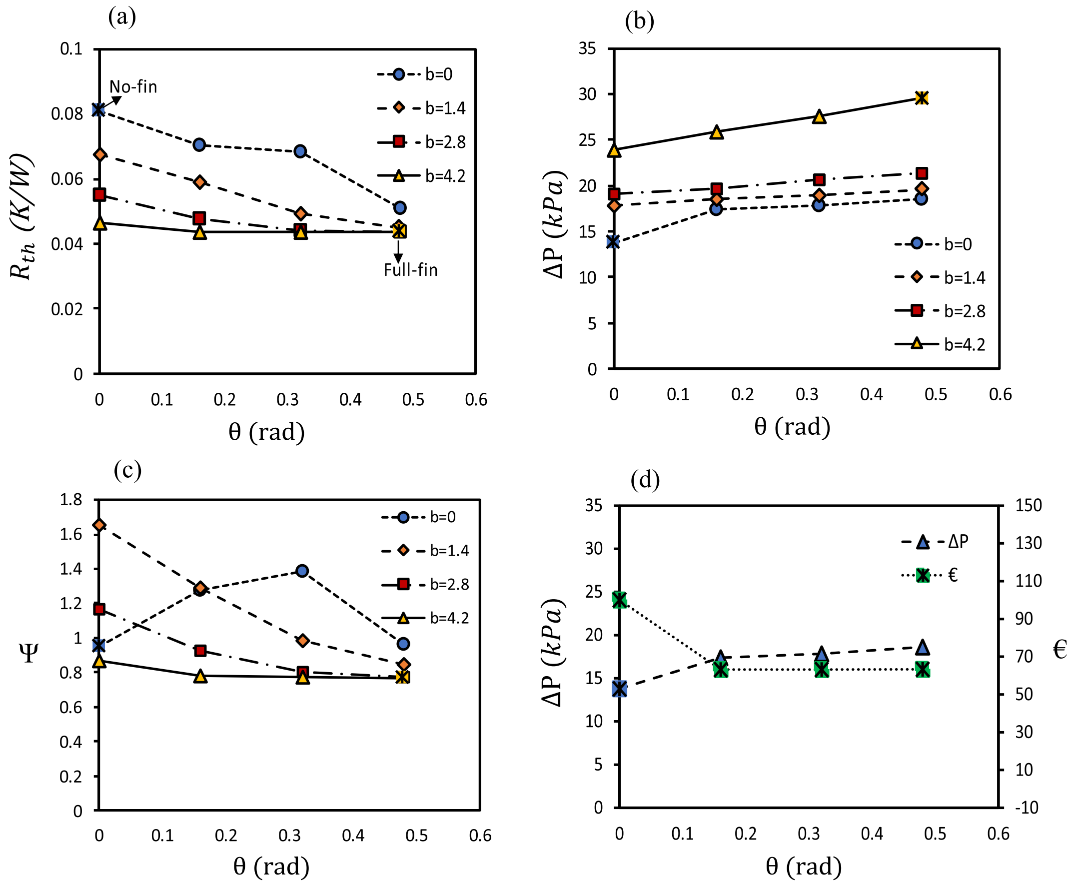

Fig. 14. The effect of the fin height profile design parameters on the (a thermal resistance. (b) pressure drop, (c) temperature distribution non-uniformity, and (d) porosity and pressure drop of designs with b = 0.

any appreciable dependency on the slope. The thermal resistance values for b = 4.20 and different profile slopes of 0 and 0.48 radians are found to be 0.0464 and 0.0438(K/W), respectively, which shows approximately a 5% reduction in thermal resistance. For the design points with b = 4.20, the variation in the profile slope value does not significantly influence the heat transfer surface area and porosity value

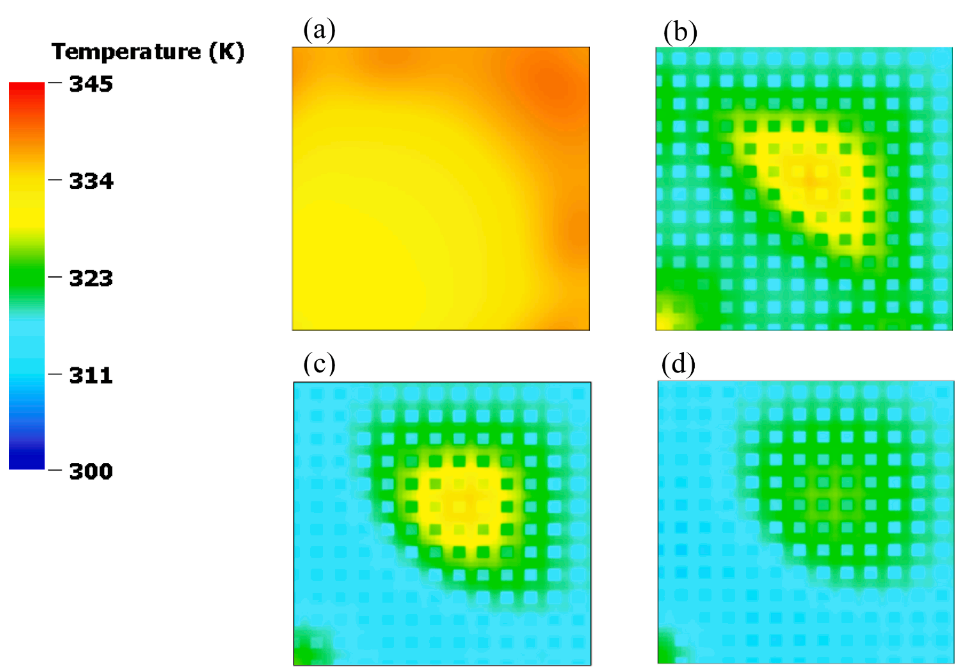

Fig. 15. Representative temperature profile on the chip surface for (a) case design with b = 0 mm, θ = 0 rad, (b) case design with b = 0 mm, θ = 0.16 rad, (c) case design with b = 0 mm, θ = 0.32 rad, (d) case design with b = 0 mm, θ = 0.48 rad.

(Fig. 14 (a)), so the effect of θ on thermal resistance is negligible. In contrast, Fig. 14(b) illustrates that for the design points with $b = 4.20$, pressure drop shows an appreciable decrease with decreasing θ. This can be attributed to the removal of fin profiles mainly in the core potential region of the impinging jet. For other b values, pressure drop has mild dependency trend with the slope. The contact surface area created by increasing θ is not in the path of the main flow. Consequently, pressure drop is weak function of θ. It is clear that the effect of θ on the pressure drop is significant when a pin fin profile with $\theta = 0.16$ and $b = 0$ is added to the no pin design. This can be explained by the fact that any reduction in porosity will augment velocity and thus pressure drop. A larger θ means there is more solid–fluid contact surface area, and thus friction, which accompanies a rise in the pressure drop value. The temperature distribution non-uniformity has similar trends with thermal resistance except for the design with $b = 0$. Fig. 15 shows the corresponding temperature profiles on the surface of the electronic chip for the designs with $b = 0$ and different profile slopes. Here, recirculation zones appear at the inlet zone. The maximum temperature occurs at the regions between the corners and the center since these regions receive less coolant flow. Based on the observations from the parametric study, any improvement in the heat transfer performance is accompanied by an increase in the pressure drop. Therefore, it is worth mentioning that properly selecting the relevant design parameters is vital to improving the cooling device's performance.

4.4. Comparison

A comparison study is carried out to evaluate the performance of the jet impingement chip-attached micro pin fin cooling device. The basis for comparison is one of the preferred industry cold plates, impingement micro channel cold plate [30,48,49]. The thermal resistance of the cold plate is calculated as 0.58 $K.\frac{cm^2}{W}$ for the flow rate of 1 LPM. It is worth mentioning that this is achieved with use of a 0.10 mm TIM at the bottom of base without the use of a spreader. Though the cooling device investigated in this study avoids using TIM or spreader, the theoretically achievable thermal resistance of predefined design with a flow rate of 1LPMis 0.26 $K.\frac{cm^2}{W}$. The chip-attached predefined design is also compared to the cold plate-version model of predefined design (Table 9). The model (3) includes a 3 mm pinned copper base substrate and 0.10 mm TIM layer. The model (4) contains a 3 mm copper spreader, 3 mm copper pinned base, and two TIM layers with thickness of 0.10 mm. It is worth mentioning that the thickness of the TIM layer is assumed to be 0.1 mm. The chip-attached design compared with other three models; the chip-attached design provides a better thermal performance while occupying less space on the circuit board. This design could be a great candidate for heterogeneous integration applications where multi-die circuit boards have restricted space. The limitation of this cooling design might be its higher pressure drop, which is due to the dense packages. However, optimizing the profile based on pin fins height can mitigate the pressure drop of the design to 37% without sacrificing the device's thermal performance. However, from manufacturing perspective, the chip attached pin fin approach requires special modern manufacturing methods such as Selective Laser Melting (SLM). Adoption of this approach for large scale production requires some alterations in the module level, system level production and assembly processes. Currently, the cost of an industrial SLM 3D printer is approximately between \$300 k-\$2M per machine depending on manufacturer and capabilities. In addition to the cost of machine procurement, material cost such as metal powder, maintenance, and operation are notable. As a result, this approach is mostly designed for high heat density applications where the conventional cold plate cooling approaches with TIMs, do not suffice and more cooling capacity is necessary to enable functionality, performance, and reliability of such high heat density processors.

Table 9
Comparison results of the chip attached design to the cold plate models.

	Design description	Schematic of design	$R_{th}\left(K.\frac{cm2}{W}\right)$
(1)	Chip-attached predefined design	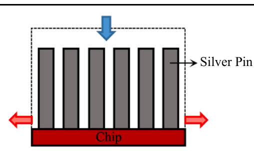	0.26
(2)	Impinging cold plate with a base and TIM	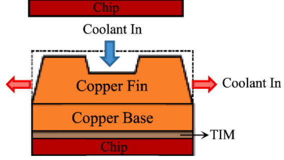	0.58
(3)	Predefined design with a base and TIM	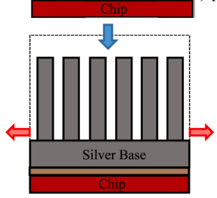	0.59
(4)	Predefined design with a base, spreader, TIMS	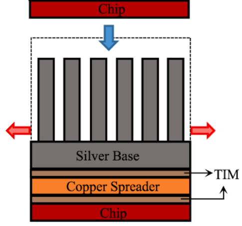	0.96

5. Concluding remarks

In conclusion, a multi-objective optimization study was performed on a novel chip-attached micro pin fin direct cooling device to minimize pressure drop and the thermal resistance. The optimization study was accomplished in two parts. In the first part, the shape optimization was performed by a traditional weighted sum approach using an iterative Jaya algorithm. Then, the same problem was solved using a more modern optimization approach, known as NSGA-II. The results of both approaches are in close agreement. In the second part, the optimization of the fin height profile is solved using an ANN combined with an elitist NSGA-II.

- Sensitivity analysis results show that fin space has a significant effect on the thermal and hydraulic performance of the design. To identify the effect of design parameters on the response parameters, parametric studies were performed using a data-based model. It was determined that properly selecting the relevant design parameters is vital for improving the cooling device's performance.
- The results of parametric study clearly show the conflicting nature of thermal resistance and pressure drop, which made it necessary to perform the multi-objective optimization study.
- Through profile optimization, it is possible to achieve a design that can mitigate pressure drop to 37% without sacrificing thermal resistance.
- The predefined chip-attached design was compared to three cold plate-versions. Compared to the cold plate-versions with a base and TIM layers, the predefined chip-attached design showed a 55% reduction in thermal resistance.
- Overall, the results showed that a chip-attached fin cooling device can provide electronic miniaturization and improved hydraulic and thermal performance in high heat flux and heterogeneous integration applications.

For further research, the experimental validation of the CFD results from this study will be performed.

Declaration of Competing Interest

The authors declare that they have no known competing financial interests or personal relationships that could have appeared to influence the work reported in this paper.

Acknowledgements

This work is supported by SRC (Task 2878.006). Many thanks to Vibhash Jha for their useful suggestions. S.N.S. acknowledges the NSF Award IIP-1738793 and the Integrated Electronics Engineering Center (IEEC) at the State University of New York at Binghamton. The IEEC is a New York State Center for Advanced Technology with funding from New York State through the Empire State Development Corporation.

References

[1] S.V. Garimella, Y.K. Joshi, A. Bar-Cohen, R. Mahajan, K.C. Toh, V.P. Carey, M. Baelmans, J. Lohan, B. Sammakia, F. Andros, Thermal Challenges in next Generation Electronic Systems - Summary of Panel Presentations and Discussions, IEEE Trans. Comp. Packag. Technol. 25 (4) (2002) 569–575.
[2] V. Venkatadri, B. Sammakia, K. Srihari, D. Santos, A Review of Recent Advances in Thermal Management in Three Dimensional Chip Stacks in Electronic Systems, J. Electron. Packag. 133 (4) (2011).
[3] K.J.L. Geisler, M. Iyengar, B.G. Sammakia, Cooling Of Microelectronic And Nanoelectronic Equipment: Advances And Emerging Research, World Scientific, 2014.
[4] M.I. Tradat, et al., An Experimental and Numerical Investigation of Novel Solution for Energy Management Enhancement in Data Centers Using Underfloor Plenum Porous Obstructions, Appl. Energy 289 (2021) 116663, https://doi.org/10.1016/j.apenergy.2021.116663.
[5] Y.M. Manaserh, M.I. Tradat, C.H. Hoang, B.G. Sammakia, A. Ortega, K. Nemati, M. J. Seymour, Degradation of Fan Performance in Cooling Electronics: Experimental Investigation and Evaluating Numerical Techniques, Int. J. Heat Mass Transf. 174 (2021) 121291, https://doi.org/10.1016/j.ijheatmasstransfer.2021.121291.
[6] "Novel Experimental Methodology for Characterizing Fan Performance in Highly Resistive Environments | IEEE Conference Publication | IEEE Xplore" [Online]. Available: https://ieeexplore.ieee.org/document/9190308. [Accessed: 22-Apr-2021].
[7] S. Alkharabsheh, J. Fernandes, B. Gebrehiwot, D. Agonafer, K. Ghose, A. Ortega, Y. Joshi, B. Sammakia, A Brief Overview of Recent Developments in Thermal Management in Data Centers, J. Electron. Packag. 137 (4) (2015).
[8] H. Martin, Heat and Mass Transfer between Impinging Gas Jets and Solid Surfaces, in: J.P. Hartnett, T.F. Irvine (Eds.), Advances in Heat Transfer, Elsevier, 1977, pp. 1–60.
[9] K. Jambunathan, E. Lai, M.A. Moss, B.L. Button, A Review of Heat Transfer Data for Single Circular Jet Impingement, Int. J. Heat Fluid Flow 13 (2) (1992) 106–115.
[10] B.W. Webb, C.-F. Ma, Single-Phase Liquid Jet Impingement Heat Transfer, in: J. P. Hartnett, T.F. Irvine (Eds.), Advances in Heat Transfer, Elsevier, 1995, pp. 105–217.
[11] J.A. Fitzgerald, S.V. Garimella, A Study of the Flow Field of a Confined and Submerged Impinging Jet, Int. J. Heat Mass Transf. 41 (8-9) (1998) 1025–1034.
[12] S.V. Garimella, R.A. Rice, Confined and Submerged Liquid Jet Impingement Heat Transfer, J. Heat Transfer 117 (4) (1995) 871–877.
[13] S.V. Garimella, B. Nenaydykh, Nozzle-Geometry Effects in Liquid Jet Impingement Heat Transfer, Int. J. Heat Mass Transf. 39 (14) (1996) 2915–2923.
[14] G.K. Morris, S.V. Garimella, Orifice and Impingement Flow Fields in Confined Jet Impingement, J. Electron. Packag. 120 (1) (1998) 68–72.
[15] C.T. Chang, G. Kojasoy, F. Landis, S. Downing, Confined Single- and Multiple-Jet Impingement Heat Transfer—I. Turbulent Submerged Liquid Jets, Int. J. Heat Mass Transf. 38 (5) (1995) 833–842.
[16] P. Naphon, L. Nakharintr, S. Wiriyasart, Continuous Nanofluids Jet Impingement Heat Transfer and Flow in a Micro-Channel Heat Sink, Int. J. Heat Mass Transf. 126 (2018) 924–932.
[17] P. Naphon, S. Wongwises, Investigation on the Jet Liquid Impingement Heat Transfer for the Central Processing Unit of Personal Computers, Int. Commun. Heat Mass Transfer 37 (7) (2010) 822–826.
[18] Saums, D., Jarrett, B., Mackie, A. C., and Ross, J., Thermal Management Materials Choices, Indium Corporation.
[19] A. Azizi, M.A. Daeumer, J.C. Simmons, B.G. Sammakia, B.T. Murray, S.N. Schiffres, Additive Laser Metal Deposition Onto Silicon for Enhanced Microelectronics Cooling, in: 2019 IEEE 69th Electronic Components and Technology Conference (ECTC), 2019, pp. 1970–1976.
[20] A. Azizi, M.A. Daeumer, S.N. Schiffres, Additive Laser Metal Deposition onto Silicon, Addit. Manuf. 25 (2019) 390–398.
[21] X.C. Tong, Advanced Materials for Thermal Management of Electronic Packaging, Springer, New York, New York, NY, 2011.
[22] K.M. Razeeb, E. Dalton, G.L.W. Cross, A.J. Robinson, Present and Future Thermal Interface Materials for Electronic Devices, Int. Mater. Rev. 63 (1) (2018) 1–21.
[23] R. Wu, T. Hong, Q. Cheng, H. Zou, Y. Fan, X. Luo, Thermal Modeling and Comparative Analysis of Jet Impingement Liquid Cooling for High Power Electronics, Int. J. Heat Mass Transf. 137 (2019) 42–51.
[24] M. Iyengar, M. Ellsworth, Design and Analysis of Direct Liquid Multi-Jet Impingement Schemes for Electronics Applications, American Society of Mechanical Engineers Digital Collection (2008) 249–256.
[25] S. Wiriyasart, P. Naphon, Liquid Impingement Cooling of Cold Plate Heat Sink with Different Fin Configurations: High Heat Flux Applications, Int. J. Heat Mass Transf. 140 (2019) 281–292.
[26] S. Ndao, Y. Peles, M.K. Jensen, Effects of Pin Fin Shape and Configuration on the Single-Phase Heat Transfer Characteristics of Jet Impingement on Micro Pin Fins, Int. J. Heat Mass Transf. 70 (2014) 856–863.
[27] "Forced Convective Heat Transfer across a Pin Fin Micro Heat Sink - ScienceDirect" [Online]. Available: https://www.sciencedirect.com/science/article/abs/pii/S0017931005002255. [Accessed: 22-Mar-2020].
[28] M. Conrad, A. Diatlov, R.W. De Doncker, Purpose, Potential and Realization of Chip-Attached Micro-Pin Fin Heat Sinks, Microelectron. Reliab. 55 (9-10) (2015) 1992–1996.
[29] M. Conrad, R.W. De Doncker, M. Schniedenharn, A. Diatlov, Packaging for Power Semiconductors Based on the 3D Printing Technology Selective Laser Melting, in: 2014 16th European Conference on Power Electronics and Applications, 2014, pp. 1–7.
[30] Y. Hadad, S. Rangararajan, K. Nemati, B. Ramakrishnann, R. Pejman, P.R. Chiarot, B. Sammakia, Performance Analysis and Shape Optimization of a Water-Cooled Impingement Micro-Channel Heat Sink Including Manifolds, Int. J. Therm. Sci. 148 (2020) 106145, https://doi.org/10.1016/j.ijthermalsci.2019.106145.
[31] Y. Hadad, V. Radmard, S. Rangarajan, M. Farahikia, G. Refai-Ahmed, P.R. Chiarot, B. Sammakia, Minimizing the Effects of On-Chip Hotspots Using Multi-Objective Optimization of Flow Distribution in Water-Cooled Parallel Microchannel Heatsinks, J. Electron. Packag. 143 (021007) (2020).
[32] C.H. Hoang, S. Rangarajan, S. Khalili, B. Ramakrisnan, V. Radmard, Y. Hadad, S. Schiffres, B. Sammakia, Hybrid Microchannel/Multi-Jet Two-Phase Heat Sink: A Benchmark and Geometry Optimization Study of Commercial Product, Int. J. Heat Mass Transf. 169 (2021) 120920, https://doi.org/10.1016/j.ijheatmasstransfer.2021.120920.
[33] P. Li, K.-Y. Kim, Multiobjective Optimization of Staggered Elliptical Pin-Fin Arrays, Numerical Heat Transfer, Part A: Applications 53 (4) (2008) 418–431.
[34] K.-T. Chiang, F.-P. Chang, Application of Response Surface Methodology in the Parametric Optimization of a Pin-Fin Type Heat Sink, Int. Commun. Heat Mass Transfer 33 (7) (2006) 836–845.
[35] K. Kasza, Ł. Malinowski, I. Królikowski, Optimization of Pin Fin Heat Sink by Application of CFD Simulations and Doe Methodology with Neural Network Approximation, International Journal of Applied Mechanics and Engineering 18 (2) (2013) 365–381.
[36] D.S. Negi, A. Pattamatta, Profile Shape Optimization in Multi-Jet Impingement Cooling of Dimpled Topologies for Local Heat Transfer Enhancement, Heat Mass Transf. 51 (4) (2015) 451–464.
[37] K. Deb, A. Pratap, S. Agarwal, T. Meyarivan, A Fast and Elitist Multiobjective Genetic Algorithm: NSGA-II, IEEE Trans. Evol. Comput. 6 (2) (2002) 182–197.
[38] "Minimizing Temperature Nonuniformity by Optimal Arrangement of Hotspots in Vertically Stacked Three-Dimensional Integrated Circuits | J. Electron. Packag. | ASME Digital Collection" [Online]. Available: https://asmedigitalcollection.asme.org/electronicpackaging/article-abstract/142/4/041109/1084430/Minimizing-Temperature-Nonuniformity-by-Optimal?redirectedFrom=fulltext. [Accessed: 22-Apr-2021].
[39] S. Rangarajan, Y. Hadad, L. Choobineh, B. Sammakia, Optimal Arrangement of Multiple Heat Sources in Vertically Stacked Two-Layer 3-D IC Using Genetic Algorithm, American Society of Mechanical Engineers Digital Collection. (2019).
[40] K. Horiuchi, A. Nishihara, K. Sugimura, Multi-Objective Optimization of Pin-Fin Heatsinks, American Society of Mechanical Engineers Digital Collection (2010) 1297–1303.
[41] A. Eghtesad, M. Mahmoudabadbozchelou, H. Afshin, Heat Transfer Optimization of Twin Turbulent Sweeping Impinging Jets, Int. J. Therm. Sci. 146 (2019) 106064, https://doi.org/10.1016/j.ijthermalsci.2019.106064.
[42] J. Zhao, S. Huang, L. Gong, Z. Huang, Numerical Study and Optimizing on Micro Square Pin-Fin Heat Sink for Electronic Cooling, Appl. Therm. Eng. 93 (2016) 1347–1359.
[43] "Phase Change Material-Based Heat Sinks: A Multi-Objective Perspective (9780367344030): Rangarajan, Srikanth, Balaji, C.: Books".
[44] Radmard, V., Hadad, Y., Azizi, A., Rangarajan, S., Hoang, C. H., Arvin, C., Sikka, K., Schiffres, S. N., and Sammakia, B., 2020, "Direct Micro-Pin Jet Impingement Cooling for High Heat Flux Applications," 2020 36th Semiconductor Thermal Measurement, Modeling Management Symposium (SEMI-THERM), pp. 1–9.
[45] R. Srikanth, C. Balaji, Experimental Investigation on the Heat Transfer Performance of a PCM Based Pin Fin Heat Sink with Discrete Heating, Int. J. Therm. Sci. 111 (2017) 188–203.
[46] R. Srikanth, P. Nemani, C. Balaji, Multi-Objective Geometric Optimization of a PCM Based Matrix Type Composite Heat Sink, Appl. Energy 156 (2015) 703–714.

[47] T.L. Bergman, F.P. Incropera (Eds.), Fundamentals of Heat and Mass Transfer, Wiley, Hoboken, NJ, 2011.

[48] Y. Hadad, B. Ramakrishnan, S. Alkharabsheh, P.R. Chiarot, B. Sammakia, Numerical Modeling and Optimization of a V-Groove Warm Water Cold-Plate, in: 2017 33rd Thermal Measurement, Modeling Management Symposium (SEMI-THERM), 2017, pp. 314–319.

[49] B. Ramakrishnan, Y. Hadad, S. Alkharabsheh, P.R. Chiarot, B. Sammakia, Thermal Analysis of Cold Plate for Direct Liquid Cooling of High Performance Servers, J. Electron. Packag. 141 (4) (2019).